# New tunnel diode for zero-bias direct detection for millimeter-wave imagers

Edward T. Croke, Joel N. Schulman, David H. Chow, Howard L. Dunlap, Kevin S. Holabird, et al.

Edward T. Croke, Joel N. Schulman, David H. Chow, Howard L. Dunlap, Kevin S. Holabird, Leslie D. Warren, Matthew A. Morgan, Sander Weinreb, "New tunnel diode for zero-bias direct detection for millimeter-wave imagers," Proc. SPIE 4373, Passive Millimeter-Wave Imaging Technology V, (21 August 2001); doi: 10.1117/12.438136

SPIE.

Event: Aerospace/Defense Sensing, Simulation, and Controls, 2001, Orlando, FL, United States

# New tunnel diode for zero-bias direct detection for millimeter-wave imagers

Edward T. Croke[a], Joel N. Schulman[a], David H. Chow[a], Howard L. Dunlap[a], Kevin S. Holabird[a], Leslie D. Warren[a], Matthew A. Morgan[b], and Sander Weinreb[b]

[a]HRL Laboratories, LLC, Malibu, CA 90265
[b]California Institute of Technology, Pasadena, CA 91125

## ABSTRACT

High-resolution passive millimeter wave imaging cameras require per pixel detector circuitry that is simple, has high sensitivity, low noise, and low power. Detector diodes that do not require bias (unlike Schottky diodes) or local oscillator input ("direct detection"), and have high cutoff frequencies are strongly preferred. In addition, they must be manufacturable in large quantities with reasonable uniformity and reproducibility. Such diodes have not been obtainable for W-band and above. We are developing zero-bias square-law detector diodes based on InAs/AlSb/GaAlSb heterostructures which for the first time offer a cost-effective solution for large array formats. The diodes have a high frequency response and are relatively insensitive to growth and process variables. The large zero-bias non-linearity in current flow necessary for detection arises from interband tunneling between the InAs and the GaAlSb layers. Video resistance can be controlled by varying an AlSb tunnel barrier layer thickness. Our analysis shows that capacitance can be further decreased and sensitivity increased by shrinking the diode area, as the diode can have very high current densities. DC and RF characterization of these devices and an estimate of their ultimate frequency performance in comparison with commercially available diodes are presented.

**Keywords:** passive millimeter-wave imaging, backward diode, tunnel diode, direct detection, zero-bias diode

## 1. INTRODUCTION

Millimeter wave detection at W-band and above has great potential for imaging under a variety of environmental conditions, such as precipitation, smoke, and dust. A limiting factor at present is the large per-pixel cost of arrays. Direct-detecting, zero-bias diodes would reduce the cost significantly, as the power, noise, and complexity penalties of local oscillators and DC biasing are avoided. We propose diodes based on Sb-heterostructures which offer a cost-effective solution at W-band. Ge backward diodes [1] and planar doped barrier (PDB) diodes [2,3] are currently used as temperature insensitive zero-bias square-law detectors with good linearity and low noise. However, Ge diodes are difficult to reproducibly manufacture, are physically fragile, and are limited to about 40 GHz. PDB diodes can operate at W-band, but to date are impossible to produce in large numbers due to the challenging doping tolerances required. We demonstrate a novel diode based on the InAs/AlSb/GaAlSb material system. The diodes have a high frequency response and are relatively insensitive to process variables. The physical basis of operation is the large asymmetry in current flow necessary for detection arising from interband tunneling between the InAs and the GaAlSb layers. RF characterization of these devices and an estimate of ultimate frequency performance are presented. Millimeter-wave detector arrays containing thousands of diodes are now feasible for the first time at W-band and above.

## 2. DIODE DESIGN

The material system studied here is the InAs/AlSb/GaAlSb nearly lattice matched combination [4]. Figure 1 shows the band alignment for the various layers. For small positive bias, electrons tunnel from the InAs through the AlSb barrier into the *p*-type GaAlSb. At larger biases, the InAs conduction band edge becomes higher than the GaAlSb valence band maximum at the interface and the current is blocked [5,6]. Negative bias induces the electrons from the GaAlSb valence band to tunnel into the InAs conduction band in a monotonically increasing manner. This asymmetry in the current flow produces the large non-linearity near zero bias desired for detection and mixing [1,7]. The substitution of tunneling through the thin AlSb barrier instead of Zener tunneling through the band gap is the critical enabling difference as compared with the conventional Esaki diode [8]. The quantities of most direct relevance are $R_J$, the junction resistance and $\gamma$, the curvature coefficient: $R_J = dV/dI$ and $\gamma = d^2I/dV^2/(dI/dV)$, at $V$=0. Typically, $\gamma$ should be as large as possible for high sensitivity. The optimum $R_J$ is usually in the 1-10 kΩ range, to maximize the signal-to-noise ratio in the operational amplifier following the detector.


Passive Millimeter-Wave Imaging Technology V, Roger M. Smith, Roger Appleby, Editors, Proceedings of SPIE Vol. 4373 (2001) © 2001 SPIE · 0277-786X/01/$15.00

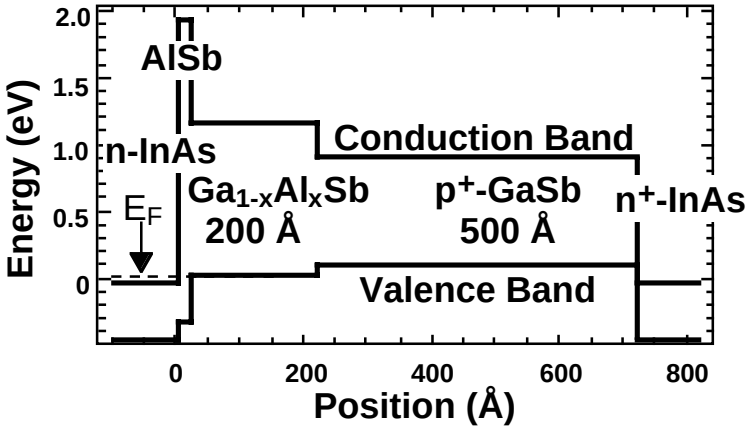


Figure 1: Band diagram for the Sb-heterostructure zero-bias diodes. Tunneling current flows from the InAs contact (left) through the AlSb barrier and is controlled by varying either the barrier thickness or the Al content in the GaAlSb blocking layer.

Mesa devices were fabricated from several samples grown by molecular beam epitaxy (MBE) on semi-insulating GaAs with different AlSb barrier thicknesses. The junction resistance, calculated by differentiating the DC *I-V* characteristics at zero bias, is plotted as a function of barrier thickness in Figure 2. A clear exponential dependence is observed, consistent with the interpretation that transport is dominated by quantum mechanical tunneling. Tunneling current flows from the InAs contact (left-hand side of Figure 1) through the AlSb barrier and is controlled by varying either the barrier thickness or the Al content in the GaAlSb blocking layer.

## 3. RF MEASUREMENTS

Diodes fabricated from sample 2519 (AlSb thickness = 30 Å) were characterized in terms of their scattering parameters and responsivity at zero bias. A small-signal equivalent circuit is derived and is used to predict the detector performance at 90 GHz.

### 3.1 Measurement Setup

The diodes were tested with a vector network analyzer and probe station. An external millivoltmeter, connected through the

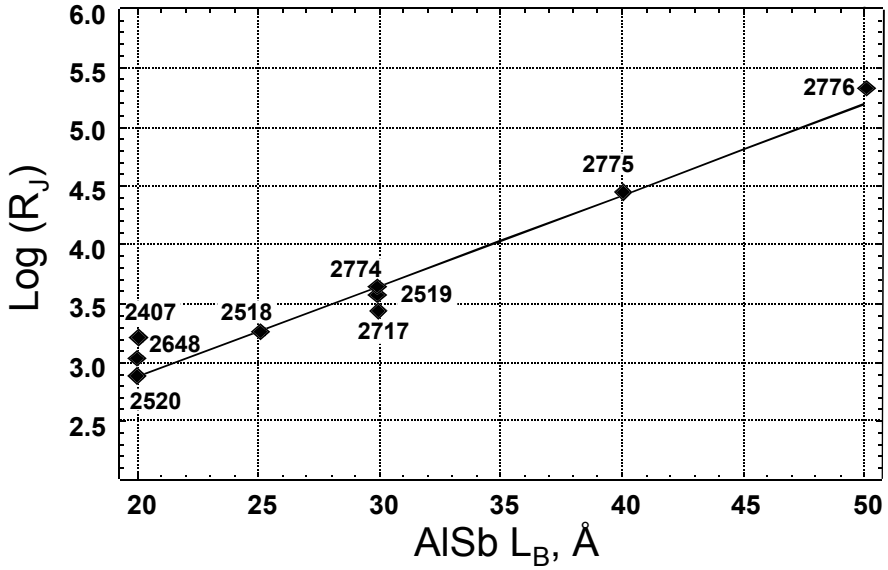


Figure 2: Measured junction resistance ($R_J$) vs. AlSb barrier thickness for several samples. $R_J$ is observed to vary exponentially with barrier thickness in a reproducible manner, permitting adjustment to suit the requirements of the particular application.

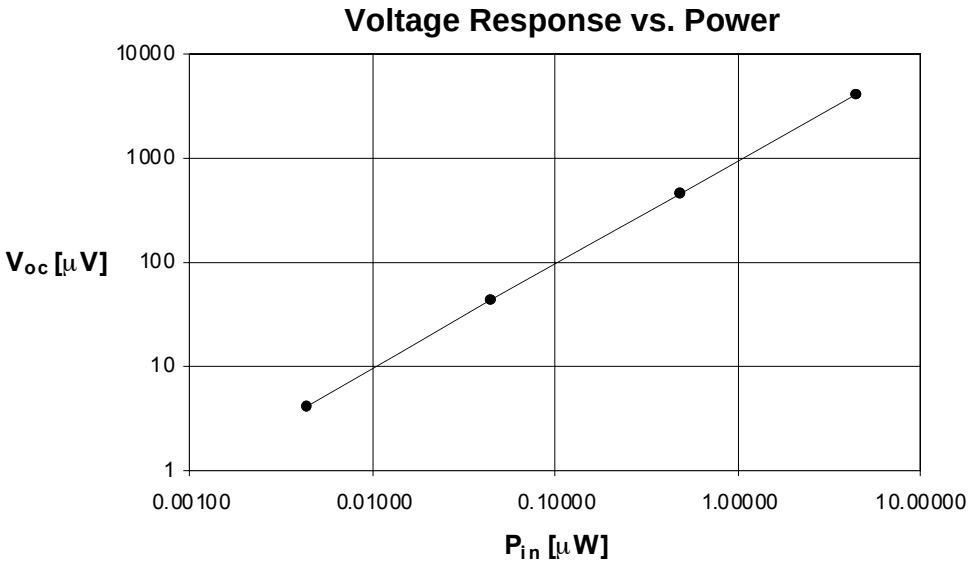


Figure 3: Open-circuit DC voltage vs. incident RF power at 10 GHz. This plot verifies that the diode was operating in its linear regime during these measurements. The diode tested was from wafer 2519.

network analyzer's bias tee, was used to monitor the DC current ($I_{sc}$) and voltage response ($V_{oc}$) of the diodes under RF drive. The power setting in the network analyzer was -15 dBm, with 0 dB attenuation, and a power slope of 0.6 dB/GHz. The power delivered to the coaxial connector on the wafer probe under these conditions was between -20 and -30 dBm from 0-50 GHz. The voltage response vs. power, plotted in Figure 3, verifies that this signal level was small enough to ensure linear operation of the diodes. The insertion loss of the wafer probe, typically about 0.5 dB, was taken into account when calculating the responsivity of the diodes.

A 1-port calibration was performed using a standard CS-5 Alumina substrate. The parasitic elements of the calibration standards on this substrate are known and were programmed into the network analyzer. This technique places the reference plane of the measurement at the tips of the wafer probe. However, the diodes on the test wafer were located at the end of a short coplanar transmission line. To account for the electrical length of this line, a port extension was entered into the network analyzer to take out the extra phase in the reflection coefficient. Using one of the on-wafer short-circuit standards as a reference, the appropriate time delay was found to be 2.5 ps, which corresponds to a 750 μm line in free space, or about 210 μm on GaAs.

**3.2 Analysis and Results**

A small-signal diode equivalent circuit (shown in Figure 4) was used to model the performance of our devices. The package capacitance, $C_P$, was determined from s-parameter measurements on unconnected diodes. $R_S$, $R_J$, and $C_J$, were determined from the real and imaginary parts of the diode impedance and the video resistance, $R_V = R_S + R_J$. The video resistance was measured at 10 and 50 GHz by taking the ratio of the open-circuit voltage ($V_{oc}$) to the short-circuit current ($I_{sc}$) under RF

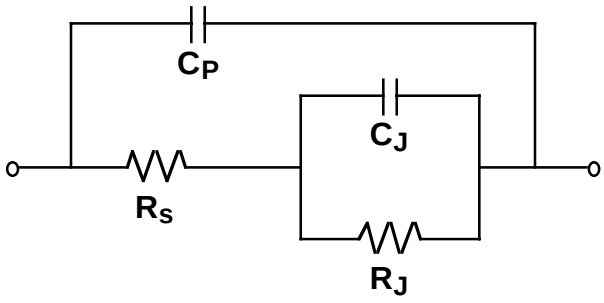


Figure 4: Small-signal equivalent circuit for the diodes. $C_P$ was determined from s-parameter measurements on unconnected diodes. $R_J$, $R_S$, and $C_J$ were calculated from the video resistance and from the real and imaginary parts of the diode impedance.

TABLE I. Model parameters and responsivity for several devices (sample 2519).

| Device ID | LxW ($\mu m^2$) | $R_S$ [Ω] | $R_J$ [Ω] | $C_J$ [fF] | $\beta_{V,meas}$ (10 GHz) [μV/μW] | $\beta_{V,meas}$ (50 GHz) [μV/μW] | $\beta_{V,opt}$ (10 GHz) [μV/μW] | $\beta_{V,opt}$ (50 GHz) [μV/μW] | $\beta_{V,opt}$ (model) (90 GHz) [μV/μW] |
|---|---|---|---|---|---|---|---|---|---|
| EXTR | 1x1 | 174 | 4580 | 7.4 | - | - | - | - | 3190 |
| EXTR | 2x2 | 43.6 | 1145 | 29.6 | - | - | - | - | 800 |
| A | 2x2 | 82.5 | 1317 | 15.6 | 1385 | 408 | 8320 ± 920 | 1390 ± 80 | - |
| B | 2x2 | 57.0 | 1540 | 13.7 | 1013 | 338 | 6985 ± 895 | 1410 ± 100 | - |
| C | 4x4 | 11.3 | 281 | 120 | 1123 | 256 | 2200 ± 60 | 472 ± 12 | 186 |
| D | 4x4 | 10.7 | 282 | 118 | 1128 | 261 | 2235 ± 62 | 498 ± 80 | 204 |
| E | 5x5 | 6.9 | 186 | 184 | 774 | 154 | 1285 ± 27 | 349 ± 12 | 131 |
| F | 10x10 | 3.5 | 50 | 693 | 154 | - | 312 ± 9 | - | 18 |

$C_P$ was taken to be equal to 13 fF for all devices. $R_J$, $R_S$, and $C_J$ were calculated using the average value of the video resistance measured at 10 and 50 GHz and from the real and imaginary parts of the diode impedance. EXTR indicates an extrapolation obtained by scaling the results for the 4x4 and 5x5 $\mu m^2$ cases linearly with area.

drive. This method was considered to be much more accurate than direct extraction from s-parameters, given the typically large values of $R_V$ compared to 50 Ω. At 50 GHz, $I_{sc}$ was too small to be measured for the largest device (10x10 $\mu m^2$) hence, only the value obtained at 10 GHz was used in calculating the model parameters. For all other devices, the average value of $R_V$ was used. This calculation was most reliable at the higher frequencies where the reactance of $C_J$ was not too large, so the final parameter values are the average of those obtained at 30, 40, and 50 GHz. These values appear in Table I.

The measured voltage responsivity, $\beta_{V,meas}$, is defined as the ratio of the open-circuit DC voltage ($V_{oc}$) to the incident RF power. This can be improved by matching the diode to the RF source. The best responsivity that can be obtained is given by:

$$\beta_{V,opt} = \frac{\beta_{V,meas}}{1 - |s_{11}|^2} \tag{1}$$

Since the intended application for these diodes is in W-band, it is interesting to predict what the performance will be at higher frequencies. Using our small signal model, the voltage responsivity into an open load can be derived in terms of the circuit elements [9] $C_P$, $R_S$, $R_J$, and $C_J$:

$$\beta_{V,opt} = \frac{R_J \gamma}{2\left(1 + R_S/R_J\right)\left(\left(1 + R_S/R_J\right) + \left(\omega C_J\right)^2 R_S R_J\right)} \tag{2}$$

where γ was determined separately from the DC *I-V* characteristics on 2x2 $\mu m^2$ devices ($\gamma = 21.7\ V^{-1}$ for sample 2519). This expression was used to model the matched voltage responsivity of the devices over the entire frequency range.

The matched responsivity, $\beta_{V,opt}$, was calculated by substituting $\beta_{V,meas}$ and $|s_{11}|$ into Equation 1, using the values of $|s_{11}|$ obtained at 10 and 50 GHz. These results are also shown in Table I. In general, $\beta_{V,opt}$ was found to be in excellent agreement with the predictions of Equation 2, using the values of the circuit elements previously obtained from the video resistance and the real and imaginary parts of the diode impedance. This close agreement can be seen in Figure 5 for devices of area 4x4 $\mu m^2$ and larger. Data appear for typical 10x10, 5x5, 4x4, and 2x2 $\mu m^2$ devices, adjusted for mismatch. The curves were generated from Equation 2 with $\gamma = 21.7$ and the model parameter values appearing in Table I. The curves representing the 2x2 and the 1x1 $\mu m^2$ cases were based on parameter values generated for the 4x4 and 5x5 $\mu m^2$ devices, assuming a linear dependence on area. The extrapolated curves show the responsivity improves dramatically as the device area decreases, exceeding 3000 μV/μW at 90 GHz.

Voltage responsivity from a commercial PDB (HP/Agilent) and a Ge Esaki diode are also plotted in Figure 5. The curve representing the performance of the PDB diode was obtained from a model provided in the technical notes for the HSCH-9161 Beamlead Detector Diode (available from HP/Agilent). For the Ge diode, we used the small-signal equivalent circuit of Figure 4 with measured values for the parameters. Clearly, the performance of the Ge diode is inferior over the entire frequency range. In fact, since the curvature coefficients of all these diodes are similar, the main cause of the variation at low

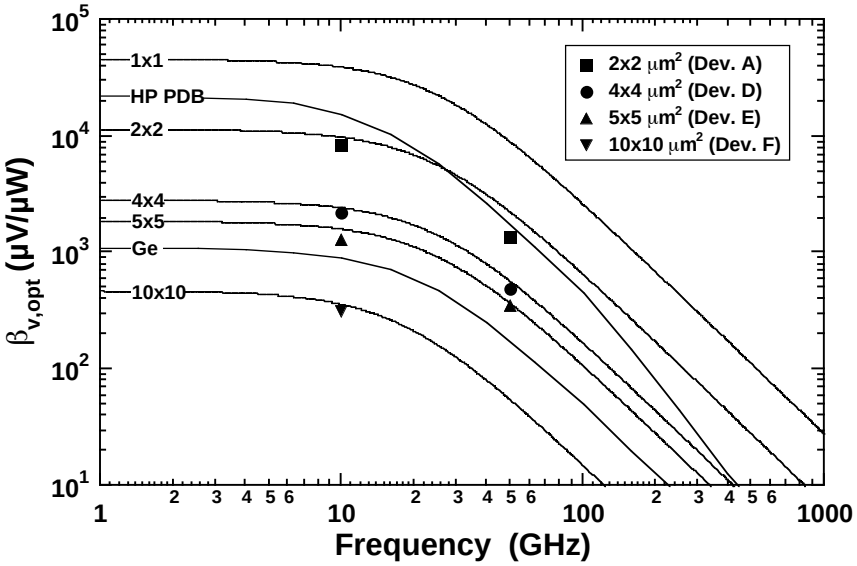


Figure 5: Voltage responsivity vs. frequency for sample 2519, compared with the commercially available planar-doped barrier diode (from HP/Agilent) and a Ge backward diode.

frequency is likely attributable to the proportionality with $R_J$, as seen in Equation 2. In particular, the HP PDB diode model has an $R_J$ of 2200 Ω, about twice that of the 2x2 diodes of sample 2519. At higher frequencies, sample 2519 is comparable or slightly better, especially when the diode area is reduced to the 1x1 $\mu m^2$ case.

At frequencies in excess of 30 GHz, the diodes operate in the tail of the frequency cutoff regime. Here, the sensitivity of the HP PDB diode is considered acceptable for 94 GHz operation, but the sensitivity is still well below the low frequency value. Even the 37 GHz sensitivity is quite degraded. Further optimization of the Sb-heterostructure diodes by further decreasing the device area makes the goal of surpassing the PDB diode at 94 GHz seem achievable.

## 4. CONCLUSIONS

InAs/AlSb/GaSb p-n Esaki backward diodes have been demonstrated which are equal or superior to Ge diodes both in their electrical and physical characteristics. S-parameter measurements indicate performance comparable to PDB diodes should be easily attainable. The flexibility of MBE provides the ability to tailor the doping profile and barrier compositions to optimize for the desired application in a reproducible way. Voltage responsivities approaching 3000 μV/μW at 90 GHz should be possible by further reducing the device area. Applications that may benefit are those requiring zero bias temperature insensitive mixing or detection with low noise and very linear square law behavior including radiometric temperature measurement and passive millimeter wave imaging.

## 5. ACKNOWLEDGEMENTS

Partial support for this work was provided by the National Reconnaissance Office under Contract No. NRO000-00-C-0071, the Army Research Laboratory under Contract No. DAAL01-94-C-0100, and Trex Enterprises Corporation.

## 6. REFERENCES

1. C. A. Burrus Jr., "Backward Diodes for Low-Level Millimeter-Wave Detection," *IEEE Transactions on Microwave Theory and Techniques* **11**, 357 (2000).
2. R. J. Malik, K. Board, L. F. Eastman, C. E. C. Wood, T. R. Aucoin, and R. Ross, "Planar Doped Barriers in GaAs by Molecular Beam Epitaxy," *Electronics Letters* **16**, 836 (1980).
3. M. J. Kearney, A. Condie, and I. Dale, "GaAs Planar Doped Barrier Diodes for Millimetre-Wave Detector Applications," *Electronics Letters* **27**, 721 (1991).

4. H. Takaoka, C.-A. Chang, E. E. Mendez, L. L. Chang, and L. Esaki, "GaSb-AlSb-InAs Multi-Heterojunctions," *Physica* **117B** & **118B**, 741 (1983).
5. L. F. Luo, R. Beresford, and W. Wang, "Interband Tunneling in Polytype GaSb/AlSb/InAs Heterostructures," *Appl. Phys. Lett.* **55**, 2023 (1989); R. Beresford, L. F. Luo, K. F. Longenbach, and W. I. Wang, "Interband Tunneling in Single-Barrier InAs/AlSb/GaSb Heterostructures," *Appl. Phys. Lett.* **56**, 952 (1990).
6. J. F. Chen, L. Yang, M. C. Wu, S. N. G. Chu, and A. Cho, "On the Effect of the Barrier Widths in the InAs/AlSb/GaSb Single-Barrier Interband Tunneling Structures," *J. Appl. Phys.* **68**, 3451 (1990); L. Y. Yang, M. C. Wu, J. F. Chen, Y. K. Chen, G. L. Snider, and A. Y. Cho, "Quantization Effect on Capacitance-Voltage and Current-Voltage Characteristics of an InAs/AlSb/GaSb Interband Tunneling Diode," *J. Appl. Phys.* **68**, 4286 (1990).
7. J. N. Schulman and D. H. Chow, "Sb-Heterostructure Interband Backward Diodes," *Electron Device Letters* **21**, 353 (2000).
8. S. M. Sze, *Physics of Semiconductor Devices*, John Wiley and Sons, New York, 1980.
9. I. Bahl and P. Bhartia, *Microwave Solid State Circuit Design*, p. 549, John Wiley and Sons, New York, 1988.

[a]croke@hrl.com; phone 1 310 317-5546; fax 1 310 317-5485; HRL Laboratories, LLC, 3011 Malibu Canyon Rd. RL63, Malibu, CA 90265; [b]mmorgan@caltech.edu; phone 1 626 395-4871; California Institute of Technology, 1201 E. California Blvd., Pasadena, CA 91125